Int J Thermophys (2009) 30:1179–1196
DOI 10.1007/s10765-009-0589-z

Two-Phase Flow Analyses During Throttling Processes

V. Vacek · V. Vinš

Received: 23 September 2008 / Accepted: 5 May 2009 / Published online: 22 May 2009

Abstract This study presents an experimental investigation of the throttling process of saturated fluorocarbon refrigerants (such as R116, R218, and R610) inside capillary tubes. For the detailed two-phase flow analyses, refrigerant R218 was selected. A divided capillary tube was prepared with a set of precise pressure and temperature sensors providing detailed information about the refrigerant flow behavior inside the tube. The metastable flow regions of the superheated liquid and of the two-phase vapor-liquid mixture were clearly detected. A correlation for the 'underpressure' of vaporization applicable for capillary flow of fluorocarbon refrigerants was determined. New experimental data were compared with a modified numerical model simulating all four capillary flow regions. A negative effect of non-condensing gases present within the cooling circuit on the overall capillary tube performance was experimentally noted.

Keywords Capillary tube · Dissolved gas · Metastable flow · Modeling · Saturated fluorocarbon · Throttling process

List of Symbols

C	Coefficient
D'	Reference length, m
Gb	Gibbs number
ID	Inner diameter, m

V. Vacek · V. Vinš
Faculty of Mechanical Engineering, Czech Technical University in Prague,
Technická 4, 166 07 Prague 6, Czech Republic

V. Vinš (✉)
Institute of Thermomechanics AS CR, v. v. i., Dolejškova 1402/5,
182 00 Prague 8, Czech Republic
e-mail: vins.vaclav@seznam.cz

k_{meta}	Lackme coefficient
K	Boltzmann constant, $1.38066 \times 10^{-34}\text{J} \cdot \text{K}^{-1}$
L	Capillary tube length, m
m	Mass, kg
$\dot{m}$	Mass flow rate, $\text{kg} \cdot \text{s}^{-1}$
n_i	Exponent ($i = 1, 2, 3$)
p	Pressure, Pa
Δp	Underpressure of vaporization ($p_{\text{sat}} - p_{\text{vap}}$), Pa
Re	Reynolds number
T	Temperature, K
ΔT	Degree of subcooling, °C
x	Vapor quality
y	Saturated state mass fraction

Greek letters

ε	Wall roughness, m
ϕ	Nucleation factor
ρ	Density, $\text{kg} \cdot \text{m}^{-3}$
σ	Surface tension, $\text{N} \cdot \text{m}^{-1}$

Subscripts

cond	Condition within condenser
cor	Correlated data
crit	Condition at critical point
exp	Experimental data
g	Gas phase
i	Index of computational grid point
in	Condition at inlet of capillary tube
l	Liquid phase
ml	Superheated liquid
sat	Saturation
sub	Subcooled liquid
vap	Vaporization

1 Introduction

Saturated fluorocarbons, referred to also as fluorinert liquids, are widely used as solvents and heat transfer media in the electronics industry. Since these substances have several outstanding properties, namely high dielectric performance, chemical stability, and radiation hardness, they can also be successfully employed as refrigerants in some special applications such as microelectronics or semiconductor particle detector cooling [1]. Saturated fluorocarbons are used as clean refrigerants with no oil contamination, usually in dry operation in such applications. R218 (perfluoropropane) and R610 (perfluorobutane) are, for instance, used in evaporative cooling circuits of

particle detectors built at the CERN laboratory; see, for example, Hallewell et al. [2], Haywood et al. [3], or Oriunno et al. [4].

1.1 Capillary Flow Studies

Over the last 20 years, many researchers have focused on detailed descriptions of the refrigerant throttling process and tried to develop precise predictive methods of capillary tube behavior. The majority of these studies deal with theoretical modeling of the capillary flow process using numerical simulation. García-Valladares et al. [5] introduced one of the most complex numerical models of capillary flow, solving both adiabatic and non-adiabatic flow cases. Xu and Bansal [6] presented another simulation of non-adiabatic refrigerant flow inside the capillary tube. Other researchers have described the effect of capillary tube coiling on mass flow rate; see, for instance, the studies of Zhou and Yufeng [7] or the additional numerical simulation of García-Valladares [8]. Several researchers have also collected large sets of experimental data measured with capillary tubes of different lengths and inner diameters. A few of them should be noted: Melo et al. [9], Kim et al. [10], Choi et al. [11], and Jabaraj et al. [12]. Dimensional analysis of the experimental data provides relatively simple and accurate predictions of the mass flow rate. However, these models should be applied only to tested refrigerants and in a relevant range of operational conditions.

In spite of the increasing number of references studying refrigerant flow through a capillary tube, there are little data for the saturated fluorocarbon refrigerants. The main motivation of this study was to perform detailed experimental investigation of the two-phase flow of saturated fluorocarbon refrigerants throttled inside a capillary tube.

Mikol [13], Koizumi and Yokoyama [14], or Li et al. [15] reported that a typical flow of clean refrigerant inside capillary tubes consists of four regions: single-phase flow of subcooled liquid, metastable flow of superheated liquid, metastable two-phase flow, and thermodynamically equilibrated two-phase flow. Two boundary regions can be relatively easily described by using basic thermodynamics' and fluid mechanics' laws. The remaining metastable regions, i.e., thermodynamically non-equilibrated phenomena, can significantly affect overall performance of the capillary tube. Unfortunately, analyses of these phenomena are still not frequently addressed in the literature.

1.2 Metastable Flow Inside a Capillary Tube

The prime variable describing metastable flow is the underpressure of vaporization, Δp, i.e., the difference in pressure at the onset of vaporization from the saturation pressure corresponding to the refrigerant temperature. There are two main approaches to deal with underpressure prediction. The first, relatively simple correlation was introduced by Lackme [16]. The absolute pressure at the onset of vaporization is determined directly from the saturation pressure,

$$p_{\mathrm{vap}} = k_{\mathrm{meta}} p_{\mathrm{sat}}. \tag{1}$$

The coefficient k_{meta} varies from 0.91 to 0.95. Lackmes' correlation, Eq. 1, was employed in many numerical simulations of capillary flow, for example, by García-Valladares et al. [5]. Nevertheless, Eq. 1 has certain limitations, since it was based on hot water data and not on measurements with refrigerants. The right choice of k_{meta} affects the overall accuracy of the simulation.

Another correlation for the underpressure of vaporization was introduced by Chen et al. [17]. They prepared a detailed model of heterogeneous nucleation within an adiabatic capillary tube. This model was verified using their previously presented experimental results [15] obtained with copper capillary tubes with two different inner diameters: 0.66 mm and 1.17 mm. The theoretical background introduced by Chen et al. can be considered as the most complex and accurate model of this phenomenon so far. Nevertheless, the model seems to be valid only for experimental data measured with refrigerant R12.

In another work [18], the authors modified the correlation of Chen et al. and extended it for application to both adiabatic and diabatic capillary tubes. Diabatic refrigerant flow was experimentally measured using specially manufactured copper capillary tubes placed in a suction line. The measurements were performed only with R134a. The suggested correlation consists of two parts: the first one related to conditions in the adiabatic capillary tube—equivalent to the correlation developed for R12—and the second one related to conditions of heat transfer between the capillary tube and the suction line.

Huerta et al. [19] experimentally investigated the effect of various parameters, mainly inlet subcooling, internal diameter, and inlet pressure, on the metastable flow of R134a and R600a. The authors also tested the impact of refrigerant oil contamination.

Given that patterns of adiabatic capillary tube behavior appear to be more common and verified, the first underpressure correlation of Chen's type used for R12 was taken as the main source of inspiration for our saturated fluorocarbon flow study.

2 Experimental Setup

The test cooling circuit working with saturated fluorocarbon refrigerant was based upon modifications of the setup described in previous work [20]. The circuit consisted of two oil-free compressors, a set of chilled water heat exchangers, a pump, a test capillary tube, a PID controlled heater, and a condenser. The refrigerant mass flow rate was measured by four different flow meters: a reference precise Coriolis mass flow meter[1] with an uncertainty of 0.5 % of reading, a turbine-type volumetric flow meter with an uncertainty of 1.0 % of reading, and a thermal-type flow sensor and a volumetric flow meter, both with an uncertainty of 1.5 % of reading.

A copper-nickel capillary tube with an inner diameter of 0.95 mm was tested at three different lengths: 5.95 m, 3.93 m, and 2.38 m. Figure 1 shows a schematic of the capillary tube with the positions of pressure transducers. The pressure taps were real-

[1] Manufacturer: Bronkhorst Cori-Tech BV, Nijverheidsstraat 2-6, NL-7261AK Ruurlo, The Netherlands; Type: CORI-FLOW.

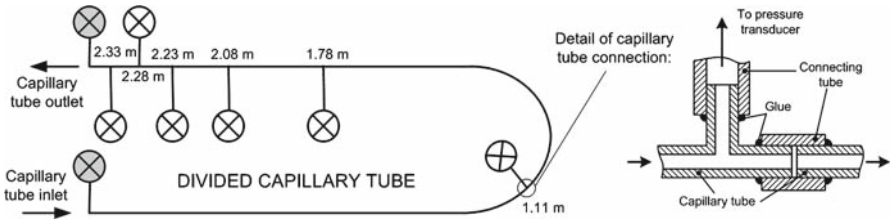

Fig. 1 Simplified schematic of divided capillary tube (2.38 m), positions of pressure transducers, and detail of connection with pressure tap

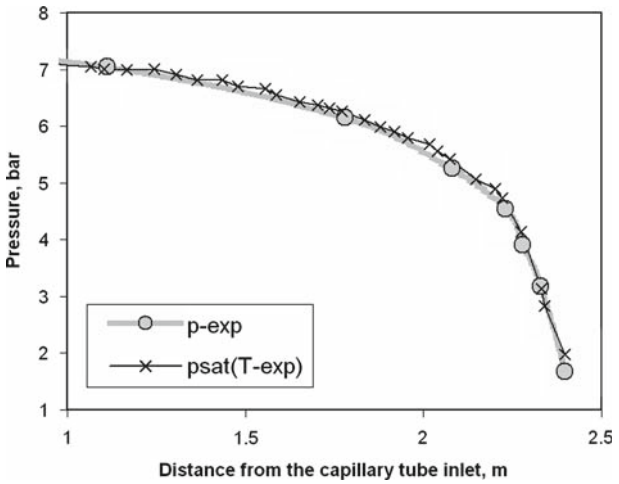

Fig. 2 Comparison of measured pressure and saturation pressure calculated from measured temperature; R218, $L = 2.38$ m, $ID = 0.95$ mm

ized by small holes drilled into the capillary tube wall approximately 3 cm from one end of each tube section. A short capillary tube piece was soldered to each hole. The capillary tube sections and the connecting tubes were glued with high-temperature resistant epoxy resin.

The test capillary tube was equipped with 37 verified temperature sensors (Kapton coated NTC, Pt1000, and Pt100) and with eight absolute pressure transducers. The temperature sensors were attached to the capillary-tube outer surface using a combination of thermal conductive paste, metal tape, and Kapton tape. The capillary tube was insulated with flexible foam insulation, which assured adiabatic flow behavior along its length. It was observed during our previous tests [20] that the temperature difference between flowing refrigerant and the outer capillary-tube surface is negligible due to the small thickness of the capillary tube (150 μm) and high thermal conductivity of copper-nickel. Figure 2 demonstrates a flow pattern with a long two-phase flow region. A comparison shows good agreement between the actual measured pressure and the saturation pressure that was determined from the recorded temperature and $p - T$ saturation curve of R218.

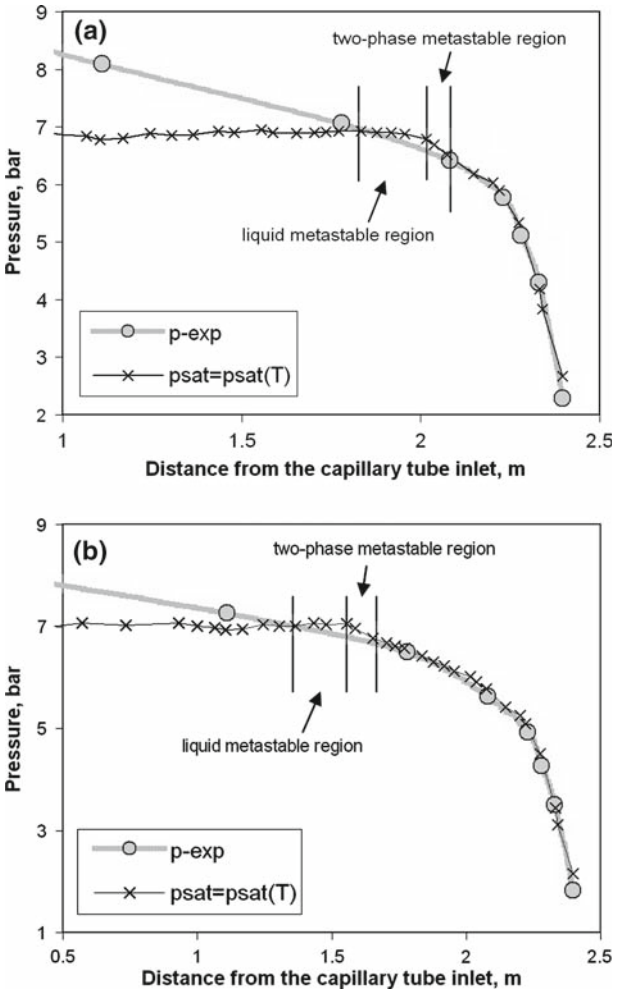

Fig. 3 Example of data measured with R218; $L = 2.38$ m, ID = 0.95 mm. Comparison of two cases with different degree of subcooling: (**a**) high degree of subcooling $\Delta T = 13.3\,^{\circ}\mathrm{C}$, $p_{\mathrm{in}} = 9.85$ bar, $T_{\mathrm{in}} = 16.5^{\circ}\mathrm{C}$, $\dot{m} = 2.82\,\mathrm{g}\cdot\mathrm{s}^{-1}$ and (**b**) low degree of subcooling $\Delta T = 5.9\,^{\circ}\mathrm{C}$, $p_{\mathrm{in}} = 8.25$ bar, $T_{\mathrm{in}} = 17.2\,^{\circ}\mathrm{C}$, $\dot{m} = 2.04\,\mathrm{g}\cdot\mathrm{s}^{-1}$

An average inner capillary diameter of 0.95 mm was measured repeating four times the weighing method [13,20] with fluorinert liquid C_7F_{16}. The relative roughness of the capillary inner wall was determined to be $\varepsilon/\mathrm{ID} = 0.0023$ with a roughness measuring device.[2]

[2] Manufacturer: Mahr GmbH, Carl-Mahr-Str.1, D-37073 Göttingen, Germany; Type: MarSurf PS1.

3 Flow of Clean Refrigerant

An example of a measured pressure profile along the capillary tube is shown in Fig. 3a, b. The absolute pressure is compared with the saturation pressure determined from the measured temperature. The capillary flow consisted of the subcooled liquid region—typical of a linear pressure drop—the two metastable regions, and the two-phase thermodynamically equilibrated region. The liquid phase persisted in the superheated condition within the metastable region, i.e., the actual pressure of the pure liquid phase was lower than the corresponding saturation pressure. The single-phase flow of superheated liquid ended at the location of the maximum underpressure $\Delta p = p_{\mathrm{sat}}(T) - p$, after which the temperature suddenly dropped. As soon as the saturation pressure started to correspond to the absolute pressure, the refrigerant flow reached thermodynamic equilibrium; $p = p_{\mathrm{sat}}(T)$.

The plotted behavior was measured at two slightly different inlet pressures and approximately the same inlet temperature of 17 °C. The lower degree of subcooling, Fig. 3b, caused the onset of vaporization further from the capillary tube outlet. The metastable region turned out to be more significant and stable, since the upstream effect of pressure fluctuations—induced by the shock waves at the capillary tube discharge—became weaker in this case. The higher mass flow rate and the onset of vaporization located closer to the capillary tube discharge concluded in stronger pressure fluctuations in the case of greater subcooling, Fig. 3a. Therefore, the metastable region was less pronounced compared to the second case shown in the Fig. 3b.

A total of 71 different measurements including distinct metastable regions were chosen for further analysis. The range of operational conditions of the refrigerant flow including the observed underpressure is listed in Table 1.

4 Correlation of Underpressure of Vaporization

Chen et al. [17] introduced a complex prediction of the underpressure of vaporization based on heterogeneous nucleation theory. The final form of the correlation is as follows:

$$p_{\mathrm{sat}} - p_{\mathrm{vap}} = \sqrt{C}\,\frac{\sigma^{3/2}}{\sqrt{K T_{\mathrm{sub}}}}\sqrt{\frac{16\pi}{Gb}}\left(\frac{\rho_{\mathrm{l}}}{\rho_{\mathrm{l}} - \rho_{\mathrm{g}}}\right) Re^{n_1/2}\left(\frac{\Delta T}{T_{\mathrm{crit}}}\right)^{n_2/2}\left(\frac{ID}{D'}\right)^{n_3/2}, \quad (2)$$

Table 1 Flow conditions of R218 in the capillary tube during the experimental tests

	p_{in} (bar)	T_{in} (°C)	$\dot{m}$ (g · s^{-1})	ΔT (°C)	Δp (bar)
min	8.08	3	1.93	5.10	0.030
max	10.61	21	3.16	21.60	0.194

where Gb marks the Gibbs number, see Chen et al. [17], and D' states the reference length given as

$$D' = \sqrt{K T_{\mathrm{sub}}/\sigma} \times 10^4. \tag{3}$$

The values of the three exponents and coefficient C in Eq. 2 were determined from an analysis of 238 sets of experimental data measured with R12: $C = 1.065, n_1 = 1.827$, $n_2 = -0.415$, and $n_3 = -6.35$. Chen et al. also showed that the non-dimensional Gibbs number remained almost constant for all experimental data collected with R12 at $\mathrm{Gb} = 38.68 \pm 2.51$. The relative error of the underpressure of vaporization predicted by Eq. 2 from the experimental data of Chen et al. was found to be approximately 26 %.

Although the correlation of Chen et al. stands on a complex theoretical background, it is limited to the sort of refrigerants and operating conditions from the experimental data of Chen et al. For instance, comparing it to experimental data of Mikol [13]—measured also with R12 but with the capillary tube having a larger inner diameter of 1.41 mm, the correlation of Chen et al. provides an underpressure of 0.16 bar which is almost three times lower than the 0.44 bar detected by Mikol. Similar differences were observed for R22 data published by Koizumi and Yokoyama [14]. Equation 2 applied to Koizumi's results gives an underpressure of 0.20 bar compared to the experimentally measured value of 0.91 bar.

4.1 Underpressure Relation for R218

The correlation, Eq. 2, of Chen et al. [17] for the underpressure of vaporization in the adiabatic capillary tube was modified for applications to the family of fluorocarbon refrigerants, i.e., R116 (perfluoroethane), R218, and R610. Collected experimental data exhibited the influence of all main flow parameters, i.e., inlet pressure, inlet temperature, and mass flow rate, on the underpressure of vaporization. The measurements were performed on three divided capillary tubes of different lengths but of the same diameter of 0.95 mm. Therefore, the effect of the inner diameter upon underpressure was not examined.

The original correlation, Eq. 2, of Chen et al. was used in a slightly modified form. The dimensionless nucleation factor was extended by the last term of Eq. 2, including the effect of the capillary tube inner diameter:

$$\phi' = \phi \left(\frac{ID}{D'} \right)^{n_3} \tag{4}$$

The exponent n_3 was considered to have the same value as by Chen et al. [17]. The introduced modification assumes that the underpressure correlation for fluorocarbon refrigerants depends also on the inner diameter. This assumption was consequently verified by comparison of the predicted underpressure to the experimental data measured and collected for several non-divided smaller diameter capillary tubes equipped only with temperature sensors distributed along their lengths.

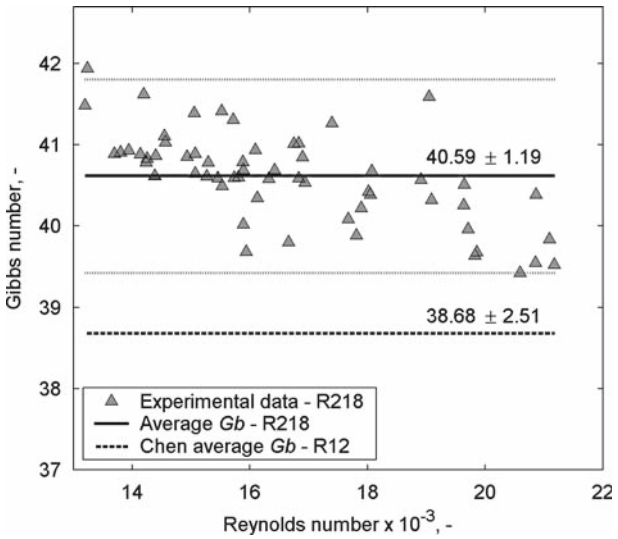

Fig. 4 Gibbs number determined from experimental data of R218 compared with result for R12 of Chen et al. [17]

As can be seen in Fig. 4, the Gibbs number did not vary much for all measured capillary flow conditions during our experiments, which agrees with the conclusion of Chen et al. The value $Gb = 40.59 \pm 1.19$ corresponding to measured R218 flow was slightly higher than the one cited by Chen et al. for R12. Nevertheless, the average falls in the Gibbs number tolerance range of Chen et al. This closeness is apparently caused by a similarity of relevant thermophysical properties of R12 and R218 in the temperature range of Chen et al. and our experimental data. The Gibbs number depends, in principle, on the viscosity and the density of saturated phases, the vapor pressure, and the surface tension. Since these quantities have comparable values for both refrigerants at the considered temperatures between 240 K and 305 K, the Gibbs number of R218 became quite similar to that of R12.

The coefficient C and two exponents n_1, n_2 were determined from 71 sets of experimental data: $C = 1.008$, $n_1 = 1.7522$, and $n_2 = -0.4577$. Equation 5 presents the final form of the underpressure correlation for fluorocarbon refrigerants:

$$p_{\mathrm{sat}} - p_{\mathrm{vap}} = 0.645 \frac{\sigma^{3/2}}{\sqrt{K T_{\mathrm{sub}}}} \left(\frac{\rho_{\mathrm{l}}}{\rho_{\mathrm{l}} - \rho_{\mathrm{g}}} \right) Re^{0.876} \left(\frac{\Delta T}{T_{\mathrm{crit}}} \right)^{0.229} \left(\frac{ID}{D'} \right)^{-3.175} . \quad (5)$$

The relative error of Eq. 5 was ± 27 %, see Fig. 5. The second data set (circles) shows the relative deviation of the original correlation, Eq. 2, of Chen et al. from our experimental data measured with R218, approximately – 40 % on average.

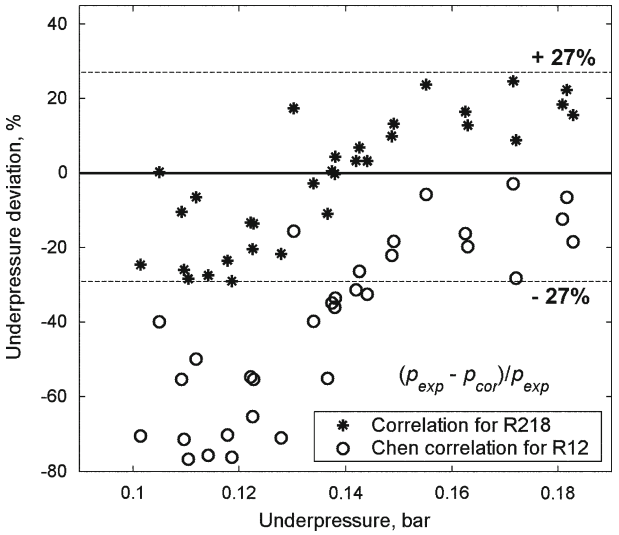

Fig. 5 Relative error of predicted underpressure of R218 by using Eq. 5 and correlation, Eq. 2, of Chen et al. [17]

4.2 Variation of Underpressure of Vaporization

Figure 6a, b shows the effects of the inlet capillary temperature and the degree of subcooling on the underpressure of vaporization of R218. Our experimental data were compared with the original correlation, Eq. 2, of Chen et al. determined for R12 and with the new relation, Eq. 5, applicable for fluorocarbon refrigerants. The measurement was performed under a constant inlet pressure of 9.05 bar. As is shown, the underpressure decreased with decreasing inlet temperature, i.e., with increasing degree of subcooling ΔT. The higher degree of subcooling evoked a longer one-phase flow region, which shifted the metastable region closer to the capillary tube outlet. The metastable flow became less significant in the location closer to the capillary tube exit due to a stronger effect of the pressure fluctuations. The predicted underpressure was in quite good agreement with the experiment, since its relative error was below $\pm$ 30 %. It should be noted that the experimental data were rather scattered due to the pressure fluctuations, which were quite significant, since the testing capillary tube had a relatively large inner diameter and quite low wall roughness ($\sim$ 2.2 μm).

The effect of varying the inlet pressure is shown in Fig. 7a, while the effect on the mass flow rate is demonstrated in Fig. 7b. This set of data corresponds to a constant inlet temperature of 17 °C. An increase in the inlet pressure caused a growth in the mass flow rate. As can be seen in Fig. 7b, the underpressure of vaporization increased with a higher mass flow, which is in agreement with conclusions of Li et al. [15]. The underpressure of vaporization was influenced by two contradictory mass flow rate effects: (a) the negative effect of pressure fluctuations caused by a higher mass flow rate and (b) the positive effect of steeper depressurization in case of an increased mass flow. The latter positive effect of the mass flow rate was stronger, since Δp increased with the higher flow rate.

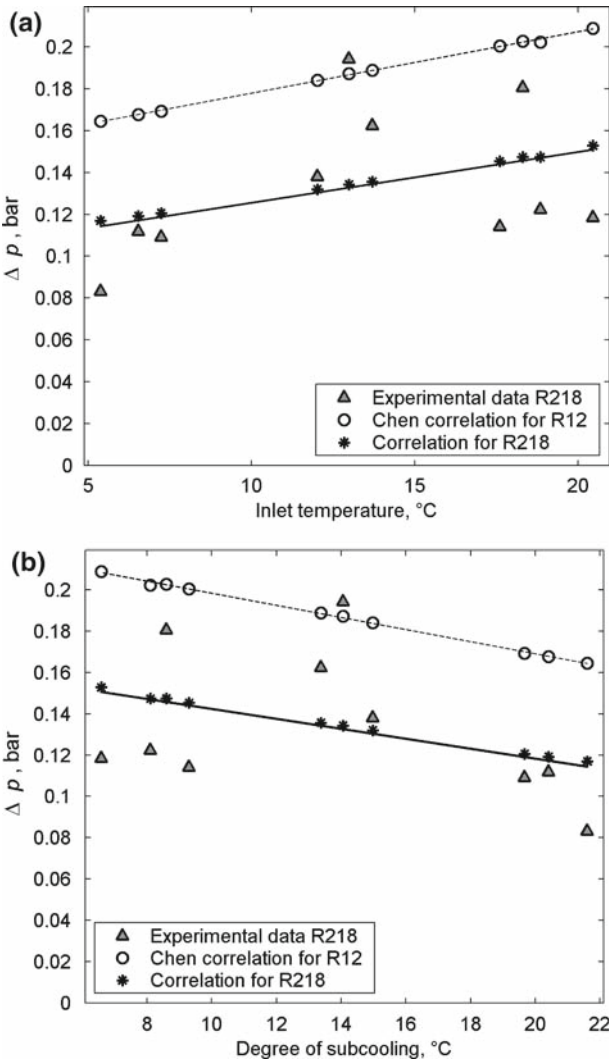

Fig. 6 Effect of (**a**) inlet temperature and (**b**) degree of subcooling on the underpressure of vaporization Δp at a constant inlet pressure of 9.05 bar and an evaporation temperature after the capillary tube around −33 °C

Slopes of the experimentally measured underpressure of vaporization are in agreement with the trends of the original correlation, Eq. 2, of Chen et al. [17] for all data shown in Figs. 6 and 7. The trend is basically shifted up by approximately 0.05 bar with regard to both experimental data of R218 and the underpressure correlation for fluorocarbon refrigerants.

5 Numerical Model with Metastable Regions

As part of this study, a numerical model described in a previous study [20] was extended by the solution of both metastable regions. The simulation was based on a solution of

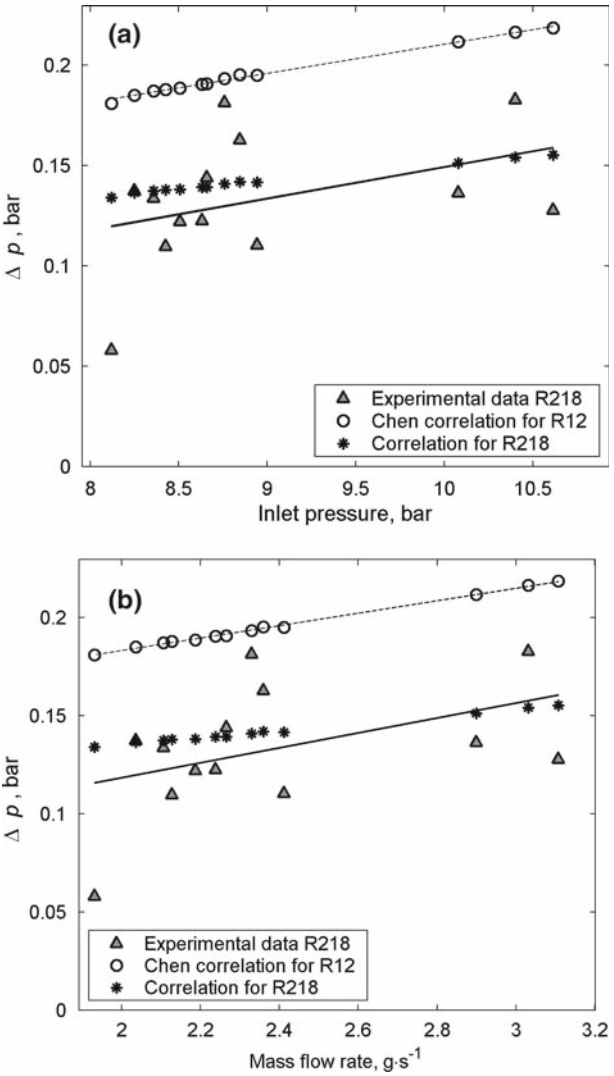

Fig. 7 Effect of (**a**) inlet pressure and (**b**) mass flow rate on the underpressure at constant inlet temperature of 17°C

two governing equations of momentum and energy. These equations were considered in a general one-dimensional form obtained by using a finite volume discretization technique. Such an approach gives a relatively simple way of subsequently adding the solutions of both the metastable flow regions. The boundary regions of the subcooled liquid flow and of the equilibrium two-phase flow are defined in the same way as in the original simulation [20].

The viscosity, density, and other properties of superheated liquid in the first *single-phase metastable region* are assumed to be the same as in the saturated liquid phase.

This simplification is possible since the fluid temperature remains constant for the case of ideal adiabatic flow. The underpressure of vaporization is calculated by the correlation, Eq. 2, of Chen et al. for R12, by Eq. 5 for fluorocarbon refrigerants and by Lackme's correlation, Eq. 1, for other refrigerants.

Similar to numerical simulations of other researchers, e.g., García-Valladares [5], *two-phase metastable flow* was assumed to have the same composition as described in Feburie et al. [21]. The two-phase metastable mixture is considered to consist of three different states: superheated liquid (ml), saturated liquid (l), and saturated vapor (g). In such a case, the vapor–liquid mixture can be described by two different mass fractions: the vapor quality,

$$x = \frac{m_{\mathrm{g}}}{m_{\mathrm{ml}} + m_{\mathrm{l}} + m_{\mathrm{g}}}, \tag{6}$$

and the mass fraction of the saturated state,

$$y = \frac{m_{\mathrm{l}} + m_{\mathrm{g}}}{m_{\mathrm{ml}} + m_{\mathrm{l}} + m_{\mathrm{g}}}. \tag{7}$$

The temperature of the superheated liquid T_{ml} is assumed to be constant, while the temperature of both saturated phases drops according to the decreasing pressure. The average temperature of the mixture in this region can be determined from

$$T = (1 - y)\, T_{\mathrm{ml}} + y T_{\mathrm{sat}}\,(p)\,. \tag{8}$$

With regard to Feburie et al. [21], the mass fraction of the saturated phase can be expressed from Eq. 9 at each computational grid point:

$$y_{i+1} - y_i - \frac{0.04}{\mathrm{ID}} \left[(1 - y_{i+1}) \left(\frac{p_{\mathrm{sat}}\,(T_{\mathrm{ml}}) - p_{i+1}}{p_{\mathrm{crit}} - p_{\mathrm{sat}}\,(T_{\mathrm{ml}})} \right)^{0.25} + (1 - y_i) \left(\frac{p_{\mathrm{sat}}\,(T_{\mathrm{ml}}) - p_i}{p_{\mathrm{crit}} - p_{\mathrm{sat}}\,(T_{\mathrm{ml}})} \right)^{0.25} \right] = 0. \tag{9}$$

In the first instance, the accuracy of the numerical model was verified by using experimental data of several conventional refrigerants from the literature. The best agreement was obtained for R12, as the precise underpressure correlation, Eq. 2, was fitted for this particular refrigerant. Figure 8a compares the numerical model with experimental data of Li et al. [22]. The capillary flow was considered as fully adiabatic. As can be seen, the predicted pressure profile was quite precise in all flow regions. The mass flow rate deviation was less than 1.0 %.

Another comparison of the simulation and experimental data of R22 measured by Koizumi and Yokoyama [14] is shown in Fig. 8b. In this case, the underpressure of vaporization had to be constrained to equal the experimentally measured value of 0.91 bar, since the underpressure of 0.20 bar determined from Chen's correlation was rather too small. Application of the relation, Eq. 2, of Chen et al. [17] derived for R12 would

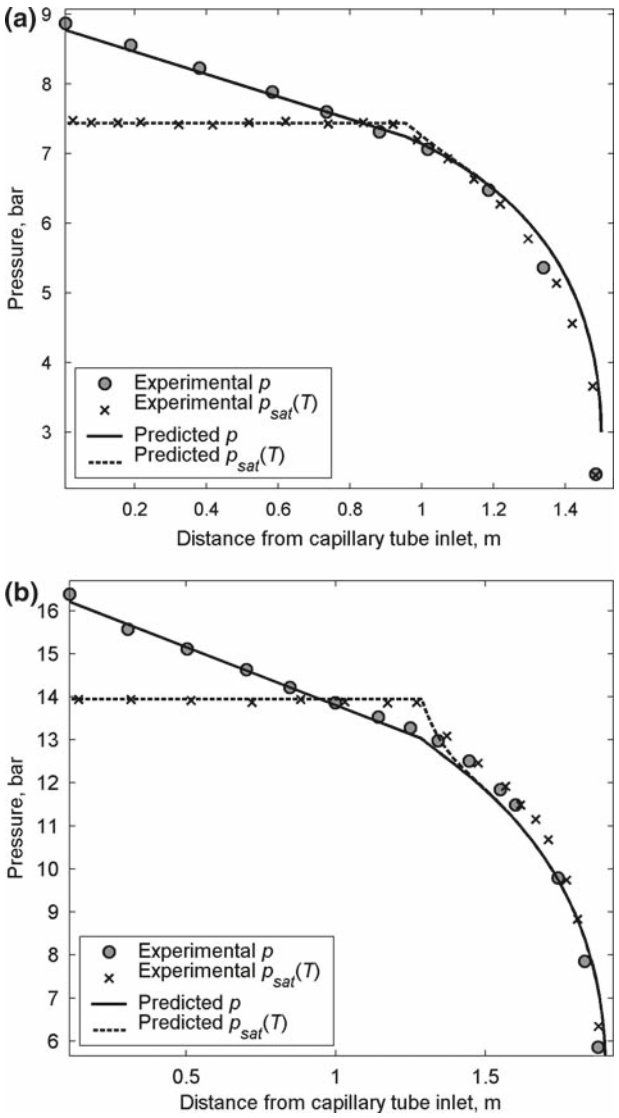

Fig. 8 Comparison of the numerical model with literature experimental data: (**a**) Li et al. [22], R12, $ID = 1.17\,\text{mm}$, $\varepsilon/ID = 0.003$, $L = 1.5\,\text{m}$, $T_{\text{in}} = 30.0\,^{\circ}\text{C}$, $\dot{m} = 4.35\,\text{g}\cdot\text{s}^{-1}$, $p_{\text{in}} = 8.85\,\text{bar}$; (**b**) Koizumi and Yokoyama [14], R22, $ID = 1.50\,\text{mm}$, $\varepsilon/ID = 0.0013$, $L = 1.9\,\text{m}$, $T_{\text{in}} = 36.1\,^{\circ}\text{C}$, $\dot{m} = 12.50\,\text{g}\cdot\text{s}^{-1}$, $p_{\text{in}} = 16.40\,\text{bar}$

lead to a significant difference in both the predicted mass flow rate and the pressure profile.

The numerical model, including Eq. 5 of the underpressure of vaporization, was compared to experimental data obtained from our measurements with fluorocarbon R218. Figure 9 shows the pressure variation of R218 under common operating condi-

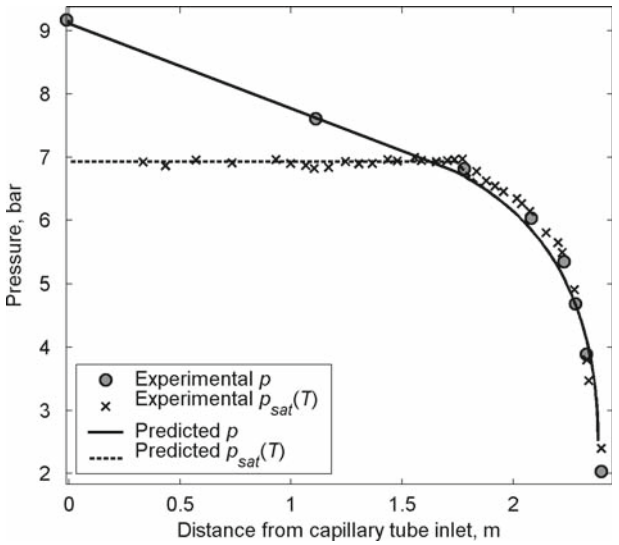

Fig. 9 Comparison of the numerical model with experimental data measured for R218. $T_{in} = 16.9\,°C$, $\dot{m} = 2.41\,g \cdot s^{-1}$, $p_{in} = 9.175\,bar$, $L = 2.38\,m$, $ID = 0.95\,mm$

tions: inlet pressure of 9.0 bar and inlet temperature of 17°C. Predicted results were in good agreement with our experiment as the mean deviation of the modeled mass flow rate was 0.9 %.

The data plotted in Fig. 10 represent the case of an enhanced inlet subcooling of approximately 21 °C. The mass flow rate obtained from the numerical simulation differed from the experiment by 2.5 %. The deviation of the predicted mass flow rate for all cases measured with R218 falls within the range of ± 3.5 %.

6 Effect of Gas Impurities

The aforementioned cooling circuit has also been used for testing other components of the evaporative cooling systems, e.g., heat exchangers, evaporators, and heaters. Every change or modification of the setup usually requires opening and consecutive closing, sealing, and vacuuming of the circuit. Even though the procedure of opening and closing the circuit has been handled with great care, the refrigerant fill was found to be contaminated by non-condensing gases after some time. The presence of gas impurities within the refrigerant is a relatively common occurrence in any evaporative cooling circuit.

In general, the non-condensing gases accumulate inside the condenser, increase the condensing pressure, and therefore lower the overall effectiveness of the cooling circuit. This feature is well known and must be avoided. However, gas impurities also affect the performance of other cooling system components. As our experimental tests have shown, even slight contamination with non-condensing gases partially dissolved in the refrigerant can slowly advance and accumulate in the whole system.

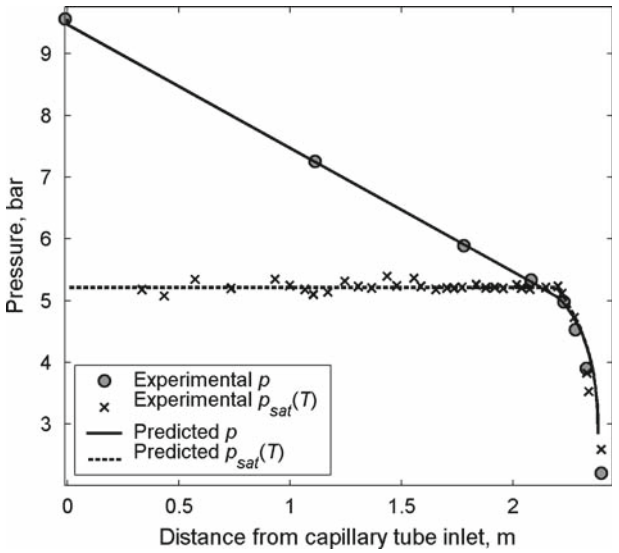

Fig. 10 Comparison of the numerical model with experimental data measured for R218. $T_{in} = 7.2\,°C$, $\dot{m} = 3.06\,g \cdot s^{-1}$, $p_{in} = 9.560\,bar$, $L = 2.38\,m$, $ID = 0.95\,mm$

Since fluorocarbon refrigerants are good solvents, the effect of gas dissolving on these substances can be quite strong. The non-condensing gases usually do not strongly impact the behavior of the liquid and the vapor single-phase flows. Nevertheless, their gas partial pressures can notably influence the two-phase flow pattern of the boiling refrigerant. An example of refrigerant flow affected by the presence of non-condensing gases is shown in Fig. 11a. A complete absence of the metastable region was detected in this case. Moreover, the onset of vaporization—typical of a temperature drop—occurred much earlier than would be expected in the case of clean refrigerant flow. The saturation pressure determined from the recorded temperature agrees well with the measured absolute pressure at the edge of fully developed equilibrated two-phase flow.

Figure 11b shows the change of the mass flow rate depending on the inlet pressure for two different refrigerant gas-contaminations. The first data (diamonds) corresponds to higher contamination, causing a difference of 0.81 bar in the real condensing pressure and the saturation pressure determined from the condensing temperature. The second data—lower contamination—(circles) were obtained at a pressure difference of 0.33 bar. The stronger gas-contamination caused a drop in the mass flow rate delivered through the capillary tube by approximately 6 %. Moreover, the presence of non-condensing gases shrank the liquid single-phase flow and consequently the mass flow rate was reduced.

7 Discussion and Conclusions

The collected experimental data, measured by using a special divided capillary tube, provided detailed information about the refrigerant flow behavior of fluorocarbon

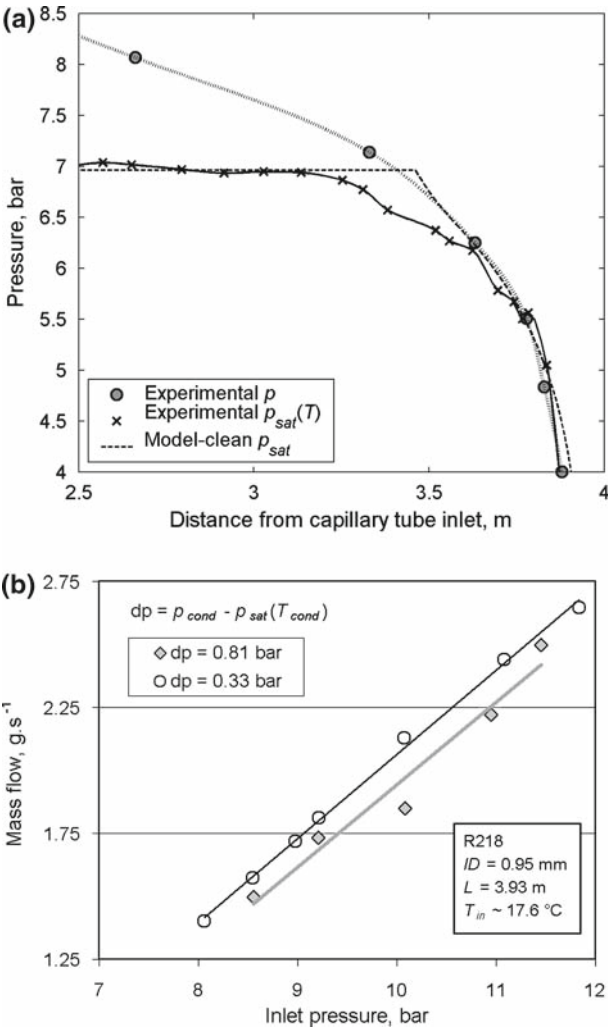

Fig. 11 (**a**) Measured pressure and saturation pressure of gas-contaminated refrigerant R218 compared with the saturation pressure of pure refrigerant predicted by the numerical model; $T_{\mathrm{in}} = 17.1\,^{\circ}\mathrm{C}$, $\dot{m}_{\mathrm{exp}} = 2.50\,\mathrm{g}\cdot\mathrm{s}^{-1}$, $p_{\mathrm{in}} = 11.45\,\mathrm{bar}$, $\dot{m}_{\mathrm{model}} = 2.66\,\mathrm{g}\cdot\mathrm{s}^{-1}$; (**b**) Influence of gas contamination—mass flow rate depending on inlet pressure at $T_{\mathrm{in}} \approx 17.6\,^{\circ}\mathrm{C}$, increasing non-condensible gas contamination is manifested by a higher value of dp inside the condenser

refrigerants within the small diameter tube. The presence of two thermodynamically metastable regions of the refrigerant flow was detected. We determined and applied correlation of the underpressure of vaporization applicable for fluorocarbon refrigerants, which is in quite good agreement with the experimental data.

New data also helped to verify the accuracy of the numerical model simulating refrigerant flow within the capillary tube by considering all four main flow regions. The difference between the predicted mass flow rate and the experiment is within $\pm$ 3.5 % and can be applied for the family of fluorocarbons used for particle detector

cooling. We believe that our experimental data collected with R218 provide a solid base for the numerical model verification, if the fluorinert refrigerant is kept clean and oil free. Besides its cooling capacity, it is also a good solvent, so the inner surface of all our tested capillary tubes was clean of eventual residuals from the capillary production process.

A prepared complex model of capillary tube behavior can be adopted (a) for the capillary dimension prediction for requested running conditions and (b) for the verification of the requested mass flow rate under a given pressure drop over the sized capillary tube. These kinds of simulations can significantly reduce the number of required experimental measurements for a cooling system equipped with multi-capillary circuits and operating at varied running conditions.

Detailed analysis of the experimental data revealed that the presence of non-condensing gases has significant negative impact on the two-phase flow pattern behavior. The gas-contamination affects the position of the onset of vaporization inside the capillary tube resulting in an overall decrease of the refrigerant mass flow rate.

A more detailed study of gas contamination, caused by non-condensing gases, is foreseen in the near future. It is desirable to implement a correction for the additional parameter (respecting Henry's law) within the simulation model of the capillary flow.

Acknowledgments The project has been supported by grants of Ministry of Education, Youth and Sports of the Czech Republic: No.: LA08015 (cooperation with CERN), LA08032 (ATLAS-CERN), CAS IAA400720710.

References

1. V. Vacek, G. Hallewell, S. Ilie, S. Lindsay, Fluid Phase Equilib. **174**, 191 (2000)
2. G. Hallewell, D. Hoffmann, V. Vacek, Int. J. Thermophys. **28**, 1730 (2007)
3. S.J. Haywood, R.L. Bates, R. Brenner, M. Doubrava, R. Fortin, M. Galuska, J. Godlewski, S. Gregory, S. Lindsay, S.J. McMahon, K. Nagai, M. Olcese, H. Pernegger, M. Stodulski, V. Vacek, P.S. Wells, J. Instrum. **3**, P05002 (2008)
4. M. Oriunno, M. Battistin, E. David, P. Guglielmini, C. Joram, E. Radermacher, G. Ruggiero, J. Wu, V. Vacek, V. Vins, Nucl. Instrum. Methods Phys. Res., A **581**, 499 (2007)
5. O. García-Valladares, C.D. Pérez-Segarra, A. Oliva, Appl. Therm. Eng. **22**, 173 (2002)
6. B. Xu, P. K. Bansal, Appl. Therm. Eng. **22**, 1801 (2002)
7. G. Zhou, Z. Yufeng, Appl. Therm. Eng. **26**, 1106 (2006)
8. O. García-Valladares, Appl. Therm. Eng. **27**, 1062 (2007)
9. C. Melo, R.T.S. Ferreira, C. Boabaid Neto, J.M. Concalves, Appl. Therm. Eng. **19**, 669 (1999)
10. S.G. Kim, M.S. Kim, S.T. Ro, Int. J. Refrig. **25**, 521 (2002)
11. J. Choi, Y. Kim, H.Y. Kim, Int. J. Refrig. **26**, 881 (2003)
12. D.B. Jabaraj, A.V. Kathirvel, D.M. Lal, Appl. Therm. Eng. **26**, 1621 (2006)
13. E.P. Mikol, ASHRAE J. **5**, 75 (1963)
14. H. Koizumi, K. Yokoyama, ASHRAE Trans. **86**, 19 (1980)
15. R.Y. Li, S. Lin, Z.Y. Chen, Z.H. Chen, Int. J. Refrig. **13**, 181 (1990)
16. C. Lackme, Int. J. Multiphase Flow **5**, 131 (1979)
17. Z.H. Chen, R.Y. Li, S. Lin, Z.Y. Chen, ASHRAE Trans. **96**, 550 (1990)
18. D. Chen, S. Lin, Int. J. Refrig. **24**, 261 (2001)
19. A.S. Huerta, F.A.S. Fiorelli, O.M. Silvares, Exp. Therm. Fluid Sci. **31**(8), 957 (2007)
20. V. Vacek, V. Vins, Int. J. Thermophys. **28**, 1490 (2007)
21. V. Feburie, M. Giot, S. Granger, J.M. Seynhave, Int. J. Multiphase Flow **19**(4), 541 (1993)
22. R.Y. Li, S. Lin, Z.H. Chen, ASHRAE Trans. **96**(1), 542 (1990)